The impact of surface plasma on the total emission charge from PZST cathode induced by nanosecond electric pulse

YANG LIU[1],[*], XUEZHONG XU[1], ZHUO XU[2], YUJUN FENG[2] and XIAOJIE LOU[3]

[1]Northwest Institute of Nuclear Technology, Xi'an 710024, China
[2]Electronic Materials Research Laboratory, Key Laboratory of the Ministry of Education and International Center for Dielectric Research, Xi'an Jiaotong University, Xi'an 710049, China
[3]Multi-disciplinary Materials Research Center, Frontier Institute of Science and Technology, and State Key Laboratory for Mechanical Behavior of Materials, Xi'an Jiaotong University, Xi'an 710049, China
*Corresponding author. E-mail: liuyang@nint.ac.cn

Abstract. Electron emission from antiferroelectric $(Pb_{0.99}Nb_{0.02})[(Zr_{0.80}Sn_{0.20})_{0.952}Ti_{0.048}]_{0.98}O_3$ cathode has been investigated. The PZST cathode can maintain a metastable ferroelectric phase by the application of a high-enough field, thus implying three possibly pulse-loading configurations for electron emission measurements. The fact that emission charge is larger than the non-compensated charge indicates that the surface plasma contributes to the total emission charge. Furthermore, χ_i (i = A, B, C), characterising the contribution of surface plasma to the total emission charge, was defined. It was found that the emission charge increases almost linearly with χ_i. Our results are of great importance for a better understanding of electron emission in antiferroelectric/ferroelectric cathodes.

Keywords. Electron emission; metastable ferroelectric; surface plasma; emission charge.

PACS Nos 77.22.Ej; 77.80.Dj; 77.84.Cg

1. Introduction

Since weak electron emission from ferroelectrics (FEs) was first reported by Miller and Savage [1] more than 50 years ago and the strong electron emission from FEs was first observed by Gundel *et al* [2] in 1989, FE cathodes have attracted much attention in the scientific community. FE cathodes, being unconventional type of cathodes, have several advantages over the conventional ones, such as instant turn-on capabilities, high emission current density (e.g. the theoretical value could be up to 10^5 A/cm^2) and so on [3–12].

However, the mechanism of electron emission from ferroelectric (FE)/antiferroelectric (AFE) materials is still unclear. Considering the potential applications of FE cathodes, an in-depth understanding of the origin of the total emission charges is particularly warranted at the current stage of research. Gundel *et al* [2,3] and Huang *et al* [13] had attributed the origin of electron emission to the change in spontaneous polarisation during electric pulse. However, Einat *et al* [11] and Rosenman *et al* [6,8] argued that the non-compensated charges on the bare FE surface induced the initially emitted electrons, which further promoted the formation of surface plasma. They believed that the reported emission charges were mainly from the surface plasma rather than the switched uncompensated polarisation bound charges [11,14,15]. Mesyats [12] and Puchkarev and Mesyats [16] considered the electron emission as a phenomenon of surface discharge from the metal–ceramics–vacuum 'triple-point junction'. Additionally, Chirko *et al* [9,10] and Shannon *et al* [17] found that the source of intense emission was indeed the plasma formed on the surface of FE ceramics.

Therefore, although FE electron emission has been studied for many years, the effect of surface plasma on the total emission charge has not yet been completely elucidated. In the present work, electron emission from a special cathode $(Pb_{0.99}Nb_{0.02})[(Zr_{0.80}Sn_{0.20})_{0.952} Ti_{0.048}]_{0.98}O_3$ (PZST80/20/4.8) has been studied in detail. Through the investigation of emission mechanism from the cathode under different pulse-loading configurations, we are able to extract the contribution of surface plasma from the total emission charge.

2. Experimental method

Polycrystalline ceramics PZST with the stoichiometric formula of $(Pb_{0.99}Nb_{0.02})[(Zr_{0.80}Sn_{0.20})_{0.952}$ $Ti_{0.048}]_{0.98}O_3$ was prepared by the conventional solid-state reaction process. To prevent lead loss during the preparation, an excess 2 wt% Pb_3O_4 was added. The mixed powders were ball milled with ZrO_2 balls for 24 h and the dried slurry was calcined at 850°C for 2 h. The dry-pressed samples were then sintered at 1300°C for 3 h in a lead-rich atmosphere to minimise the loss of lead due to volatilisation. In order to measure the electron emission, 0.5 mm PZST ceramic pellets were electroded with a full electrode on one side and a grid pattern on the opposite side, which is described elsewhere [18].

The crystal structure of the sintered samples was determined by X-ray diffraction (X' Pert PRO) with CuK$_\alpha$ radiation. The hysteresis loops (*P–E* loops) of the PZST ceramics were determined with a sine waveform of 1 Hz in a silicon oil bath at room temperature (25°C) by using a Sawyer–Tower circuit (TF analyser 2000). The home-designed set-up for measuring the electron emission from PZST cathodes is shown in figure 1 and the detailed description is given elsewhere [18]. Note that our electron emission experiment is entirely different from the charge–discharge properties of ceramic capacitors.
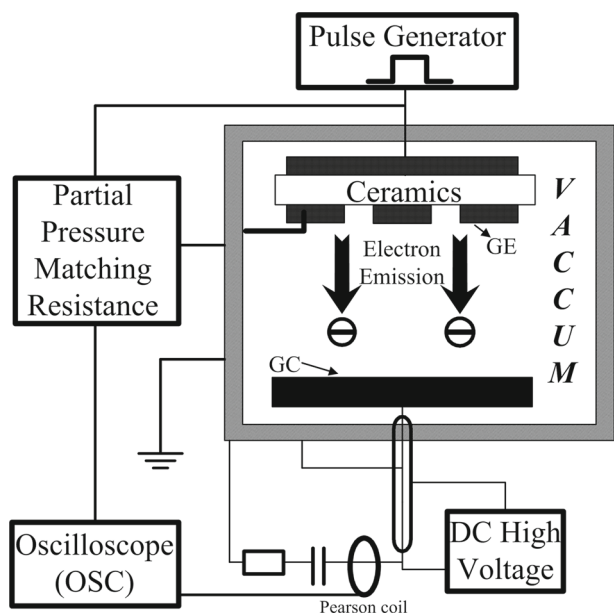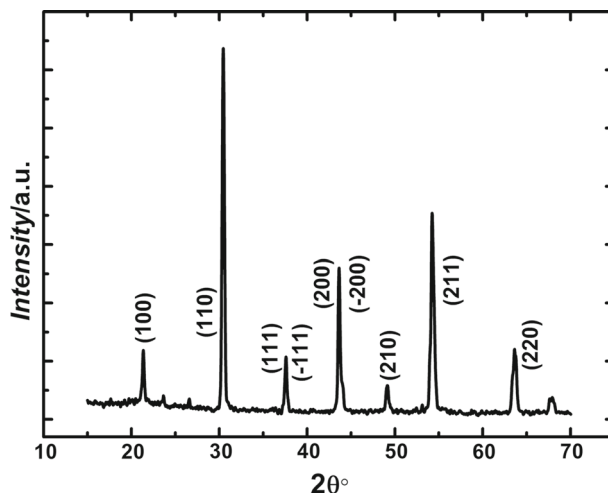
Figure 2. X-ray diffraction pattern of virgin PZST80/20/4.8 sample in the 2θ range of 15°–70°.

3. Experimental results and discussion

First of all, as shown in figure 2, the X-ray diffraction pattern of the virgin sample shows that virgin PZST80/20/4.8 possesses a pure tetragonal structure, i.e. the initial phase of PZST80/20/4.8 is AFE phase. Figure 3 shows the first-cycle *P–E* loop of the PZST80/20/4.8 ceramics at room temperature, which indicates that the virgin phase of the PZST ceramic is AFE, not FE (see O–A, figure 3). When the loading field is larger than the critical field E_{AFE-FE}, the initial AFE phase can be transformed into FE phase (see A–B, figure 3) and maintains FE even though the electric field is removed (see C–D, figure 3). Therefore, this special composition which is neither AFE nor traditional FE, is called metastable FE (see figure 3, for more details, please refer to [19–21]). In the metastable FE phase, the crucial field E_{AFE-FE} can be determined to be 37 kV/cm and its key parameters are shown as follows: the saturated polarisation $P_s = 38.3$ $\mu C/cm^2$, the remnant polarisation $P_r = 33.3$ $\mu C/cm^2$ and the coercive electric field $E_c = 10.3$ kV/cm (see figure 3). Note that E_c is smaller than E_{AFE-FE}, which is one of the most significant features of the metastable FE ceramics [19,20]. In the past, it was found that the field-induced FE PZST90/10/4 ceramics could be depolarised into an AFE phase under a shock wave or quasistatic pressure, and therefore could be used in pulse power technology [22,23]. PZST80/20/4.8 ceramics, whose properties are similar to those of PZST90/10/4, therefore could also find potential applications in shock-activated power devices.

Because of its idiosyncratic phase transition, only one PZST80/20/4.8 cathode can be triggered by three pulse-loading configurations. As shown in figure 4,

Figure 1. Experimental set-up for measuring electron emission from PZST cathodes.

configuration A is the one in which PZST80/20/4.8 is in a stable AFE phase (the original phase) under a positive pulse. Configuration B is the one in which PZST80/20/4.8 is in a metastable FE phase after the application of a high-enough electric field. For configuration B, the orientation of the induced FE polarisation and that of the positive triggering pulse point to the same direction, and therefore there is no or less polarisation switching. Configuration C is the same as configuration B except that the orientation of the induced FE polarisation and that of the positive pulse point to the opposite directions. Apparently, polarisation switching induced in configuration C is much more intensive than that in configuration B.

Figure 5 shows the typical emission current waveforms of the PZST80/20/4.8 cathodes upon the application of a positive triggering pulse of 40 kV/cm in magnitude under configuration A (figure 5a), configuration B (figure 5b) and configuration C (figure 5c). Firstly, our investigation published elsewhere

Figure 3. First-cycle *P–E* hysteresis loops of the virgin PZST80/20/4.8 ceramics at room temperature and the corresponding status.

has shown that the electric field at the metal–ceramics–vacuum triple-point can be roughly estimated to be $E = \varepsilon_r \times U/\delta$, where ε_r, U and δ are the high-field relative permittivity (not dielectric constant of the ceramic), the triggering voltage and the thickness of the cathode, respectively [6,16,18]. For the value of high-field relative permittivity, it is demonstrated that configuration C possesses the highest value and configuration A, the smallest value [18]. A configuration with lower value could be charged quickly, causing the rising edge of the triggering-field waveform to be steeper. In contrast, configuration C with the highest high-field relative permittivity leads to its triggering-field curve increasing gently, not letting the curve to be a perfect square. Secondly, due to surface flashover, one can see a sharp spike in every triggering-field curve. Surface flashover will start immediately at the triple-point junction when the cathode is triggered and the horizontal component of the electric field at the grid electrode may suppress the formation of flashover discharge, which ensures that the actual field seen at the cathode is our preset value [4,24].

About configuration A, the triggering field of 40 kV/cm is high enough to induce a very rapid macroscopic polarisation at the triple-point junction, leading to the appearance of non-compensated charges near this region [18,24]. Moreover, we expect that non-compensated charges existing in the triple-point junction can result in a strong electrostatic field at the surface of the cathode, which further induces local field emission and produces primary emission electrons for the formation of surface plasma. After that, the emission electrons induced by non-compensated charges and those from the surface plasma give rise to the formation of the emission peak, as shown in figure 5a.

For configurations B and C, the cathode is in a field-induced metastable FE phase, which can result in a fast nanosecond polarisation reversal at the falling edge of the triggering pulse [8]. Therefore, both non-compensated electrons and plasma electrons are pulled
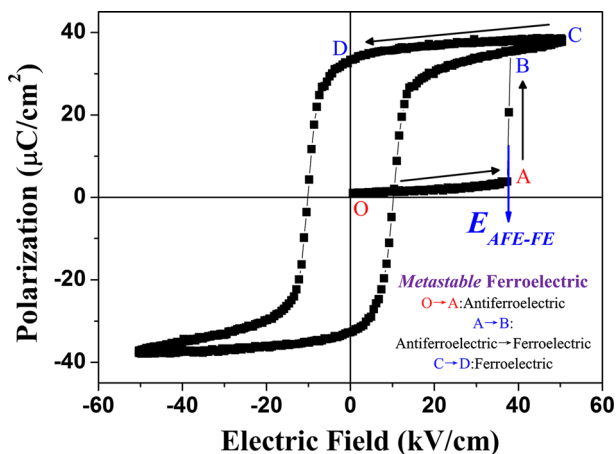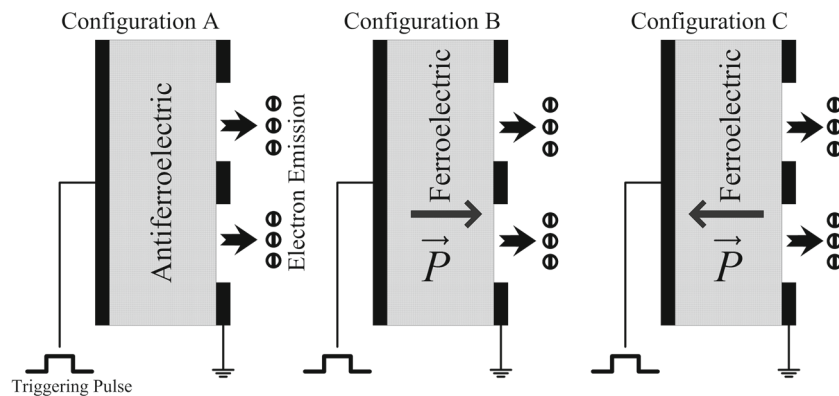
Figure 4. Schematic diagram of three different pulse-loading configurations.
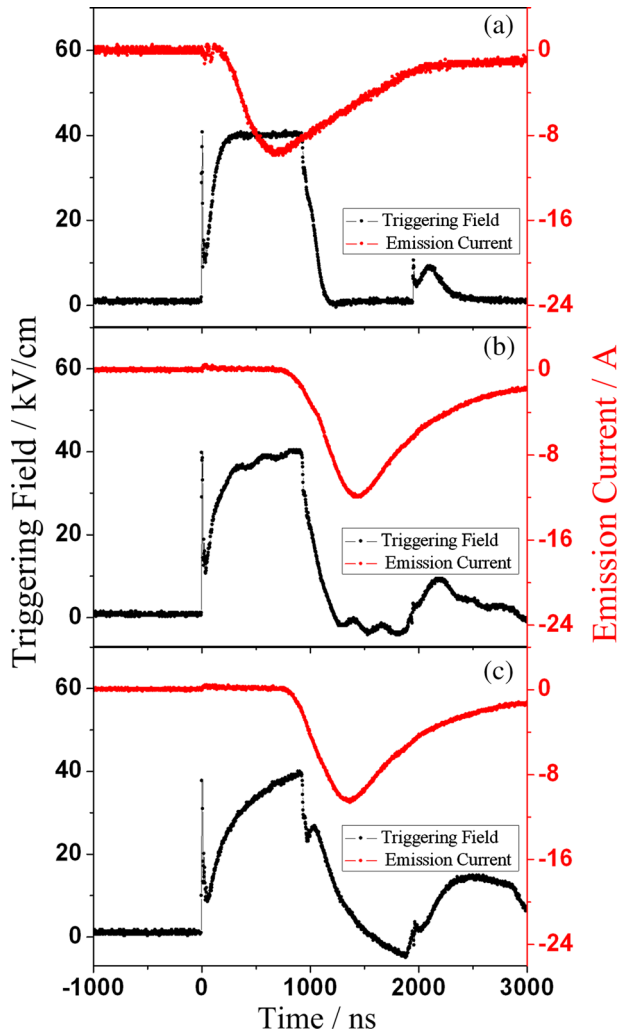
Figure 5. Emission current waveforms induced by applying a positive triggering pulse of 40 kV/cm in magnitude to the rear electrode of the PZST80/20/4.8 cathode under (**a**) configuration A, (**b**) configuration B and (**c**) configuration C.

out from the grid electrode, leading to the formation of electron emission peaks appearing at the end of the triggering pulse (see figures 5b and 5c). Furthermore, as shown in figures 5b and 5c, the delay time (the time between the emission current peak and the start of the triggering pulse) of 1361 ns in configuration C is smaller than that in configuration B (1426 ns). This may be due to the fact that in configuration C the positive pulse and the spontaneous polarisation point to different directions, which can lead to a large-scale polarisation switching, and consequently more non-compensated charges. And then, more non-compensated charges in configuration C make the electron emission to occur faster than that in configuration B. In conclusion, because of the local field emission in configuration A, its emission current peak locates at the platform area of triggering pulse, and polarisation reversal makes emission

current peaks of the other two configurations to appear at the end of the triggering field. Our results and conclusions shown are the same as those previously reported by other researchers [8,15,25].

The total emission charge, the integral of the emission current waveform over time (see figure 5), is very important for understanding the performance of FE cathodes (which require larger emission charges) and insulators (which require lower emission charges to avoid surface flash-over) [26,27]. From figures 5a–5c, the emission charge of each configuration can be obtained: the emission charge of configuration A is 1.181×10^{-5} C, that of configuration B is 1.353×10^{-5} C and that of configuration C is 1.128×10^{-5} C. That is, the total emission charges of three configurations are different though PZST80/20/4.8 with the same composition was tested under the same triggering pulse.

The non-compensated charge Q_n can be written as

$$Q_n = \Delta P_i \cdot S, \tag{1}$$

where ΔP_i ($i = A, B, C$) is the variation in polarisation during the triggering field in three different configurations and S is the effective emission area of the cathode. The effective emission area of FE cathodes is considered to be the area of the bare FE surface with the grid patterned electrode [8,16]. With respect to ΔP_i ($i = A, B, C$), the variation in polarisation induced by unipolar field is P_s for configuration A, $P_s - P_r$ for configuration B and $P_s + P_r$ for configuration C. On the other hand, the triggering field of the triple-point region is much larger than E_{AFE-FE} and/or E_c, the domains at these special regions are prone to reversal during the pulse. Thus, ΔP_i ($i = A, B, C$) during the electric pulse can be regarded as

$$\Delta P_A = \eta_A \cdot P_s,$$
$$\Delta P_B = \eta_B \cdot (P_s - P_r),$$
$$\Delta P_C = \eta_C \cdot (P_s + P_r), \tag{2}$$

where η_i ($i = A, B, C$) represents the ratio of the reversed domains to the total domains in each configuration. The triggering field is weak and short, which could not induce all the polarisation reversal of our cathode, the electric field in the triple-point junction is high enough for polarisation reversal at this special region. That is to say, $0 < \eta_i$ ($i = A, B, C$) ≤ 1. Moreover, it is obvious that the grid electrode (i.e. the triple-point junction) at any configuration is uniform, which can lead to $\eta_A = \eta_B = \eta_C$ during the nanosecond pulse.

By comparison, it was found that the total emission charge is larger than non-compensated charges for all the configurations, which indicates that the emission charge is not determined by the non-compensated charge only. It is well known that emission electrons come from two

sources: (i) non-compensated charges (the amount is determined by polarisation switching) and (ii) surface plasma. It is obvious that priming electron (electron that is first emitted from the cathode) and a tangential electric field can move intense plasma along the dielectric surface, thus the plasma density has no relationship with different pulse-loading configuration mentioned above. In order to evaluate the contribution of surface plasma to the total emission charge, a new parameter χ_i ($i = $ A, B, C), the ratio of the emission charge originated from the surface plasma to the total emission charge, is defined. Lower χ_i means that electron emission is primarily dependent on the non-compensated charge induced by polarisation switching, while higher χ_i indicates that emission charges are mainly from the surface plasma to the cathode surface.

This new parameter χ_i ($i = $ A, B, C) can be expressed as

$$\chi_A = \frac{Q_A - Q_n}{Q_A} = \frac{Q_A - \Delta P_A \cdot S}{Q_A}$$
$$= 1 - \frac{\eta_A \cdot P_s \cdot S}{Q_A}, \tag{3}$$

$$\chi_B = \frac{Q_B - Q_n}{Q_B} = \frac{Q_B - \Delta P_B \cdot S}{Q_B}$$
$$= 1 - \frac{\eta_B \cdot (P_s - P_r) \cdot S}{Q_B}, \tag{4}$$

$$\chi_C = \frac{Q_C - Q_n}{Q_C} = \frac{Q_C - \Delta P_C \cdot S}{Q_C}$$
$$= 1 - \frac{\eta_C \cdot (P_s + P_r) \cdot S}{Q_C}. \tag{5}$$

Through the discussion above, we can suppose $\eta_A = \eta_B = \eta_C = 1$ so that the analysis is easier. Hence, $\chi_A = 0.514$, $\chi_B = 0.946$ and $\chi_C = 0.048$ can be obtained through eqs (3)–(5). In the same manner, $\chi_A = 0.62$, $\chi_B = 0.96$ and $\chi_C = 0.23$ can be obtained for the PZST90/10/4 cathode [18].

Figure 6 shows the total emission charge Q_i ($i = $ A, B, C) as a function of χ_i ($i = $ A, B, C) for both PZST80/20/4.8 and PZST90/10/4 cathodes. First of all, one can see that for PZST80/20/4.8 or PZST90/10/4, χ_B is the largest, χ_C is the smallest and χ_A sits somewhere in the middle. In configuration A, the AFE–FE phase transition of the PZST cathode produces non-compensated charges for electron emission. Nevertheless, $\chi_A > 0.5$ indicates that the surface plasma is still the primary source of emission charges in configuration A. In configuration B, however, as the triggering pulse is of the same direction as that of the original polarisation, it only induced very weak polarisation switching, making the surface plasma to be almost the only source of emission charges. Therefore, in
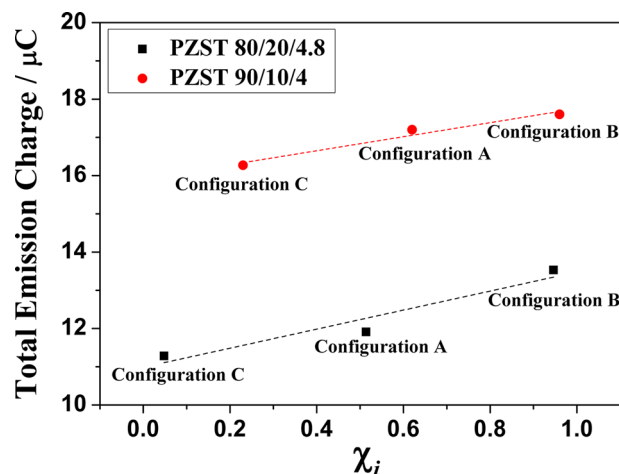
Figure 6. Total emission charge Q_i ($i = $ A, B, C) as a function of χ_i ($i = $ A, B, C) for the PZST80/20/4.8 and PZST90/10/4 cathodes.

configuration B, χ_B is approximately 1. In configuration C, the origin of emission charges is mainly from the non-compensated charges induced by large-scale FE polarisation reversal, and this results in the smallest χ_i.

Then, the results in figure 6 have been fitted using straight lines. Clearly, one sees that the total emission charge increases almost linearly by increasing χ_i. That is to say, the higher χ_i, the larger the emission charge will be. The role of surface plasma can be considerably enhanced by minimising the degree of polarisation switching. The observations in this work are useful for finding a way to enhance the total emission charges and may provide deep insight into the origin of electron emission in FE/AFE cathodes. Our findings, therefore, are of great importance for designing FE cathodes with superior properties.

4. Conclusion

In summary, strong electron emission was successfully obtained with PZST80/20/4.8 ceramics under three pulse-loading configurations. For each configuration, both polarisation switching and surface plasma contribute to the total emission charges. A new parameter χ_i ($i = $ A, B, C) characterising the contribution of surface plasma to emission charges is defined. It is found that the contribution of surface plasma to electron emission could be significantly enhanced by increasing χ_i, which further gives rise to more emission charges (see figure 6). Our results emphasise the important role the surface plasma plays in electron emission, and are of great importance for obtaining a better

understanding of the mechanism of electron emission in FE/AFE cathodes.

Acknowledgements

References

[1] R Miller and S Savage, *J. Appl. Phys.* **31**, 662 (1960)
[2] H Gundel, H Reige, E J N Wilson, J Handerek and K Zioutas, *Nucl. Instrum. Methods A* **280**, 1 (1989)
[3] H Gundel, H Riege, J Handerek and K Zioutas, *Appl. Phys. Lett.* **54**, 2071 (1989)
[4] Z X Sheng, Y J Feng, Z Xu and X L Sun, *J. Mater. Sci.* **44**, 556 (2009)
[5] M Yaseen, X J Lou, X F Chen, W Ren, Y Liu, Y J Feng, P Shi and X Q Wu, *Appl. Phys. Lett.* **104**, 222913 (2014)
[6] G Rosenman, D Shur, K Garb, R Cohen and Y E Krasik, *J. Appl. Phys.* **82**, 772 (1997)
[7] H Riege, I Boscolo, J Handerek and U Herleb, *J. Appl. Phys.* **84**, 1602 (1998)
[8] G Rosenman, D Shur, Y E Krasik and A Dunaevsky, *J. Appl. Phys.* **88**, 6109 (2000)
[9] K Chirko, Y E Krasik, J Felsteiner and A Sternlieb, *J. Appl. Phys.* **92**, 5691 (2002)
[10] K Chirko, A Sayapin, Y E Krasik and J Felsteiner, *Vacuum* **77**, 385 (2005)
[11] M Einat, E Jerby and G Rosenman, *IEEE Trans. Microw. Theory Tech.* **50**, 1227 (2002)
[12] G A Mesyats, *Phys.-Usp.* **51**, 79 (2008)
[13] X D Huang, Y J Feng and S Tang, *Acta Phys. Sin.* **61**, 087702 (2012)
[14] V D Kugel, G Rosenman, D Shur and Y E Krasik, *J. Appl. Phys.* **78**, 2248 (1995)
[15] D Shur, G Rosenman and Y E Krasik, *Appl. Phys. Lett.* **70**, 574 (1997)
[16] V F Puchkarev and G A Mesyats, *J. Appl. Phys.* **78**, 5633 (1995)
[17] D N Shannon, P W Smith, P J Dobson and M J Shaw, *Appl. Phys. Lett.* **70**, 1625 (1997)
[18] Y Liu, X J Lou, Z Xu, H L He and Y J Feng, *Ceram. Int.* **40**, 11057 (2014)
[19] T Q Yang and X Yao, *Ceram. Int.* **34**, 715 (2008)
[20] C H Zhang, Z Xu, J J Gao, C J Zhu and X Yao, *Chin. Phys. B* **20**, 097702 (2011)
[21] P Yang and D A Payne, *J. Appl. Phys.* **80**, 4011 (1996)
[22] D D Jiang, J M Du, Y Gu and Y J Feng, *J. Appl. Phys.* **111**, 024103 (2012)
[23] D D Jiang, Y J Feng, J M Du and Y Gu, *High Press. Res.* **31**, 436 (2011)
[24] Z X Sheng, Y J Feng, Z Xu and X L Sun, *Nucl. Instrum. Methods A* **593**, 539 (2008)
[25] G A Mesyats, *IEEE Trans. Elec. Insul.* **2**, 272 (1995)
[26] H C Miller, *IEEE Trans. Elec. Insul.* **28**, 512 (1993)
[27] S Beeson, J Dickens and A Neuber, *Phys. Plasmas* **20**, 093509 (2013)